WEP Warwick Evans Publishing

International Journal of Computer Science and Information Technology

ISSN: 3005-9682 (Print), ISSN: 3005-7140 (Online) | Volume 8, Number 1, Year 2026
DOI: https://doi.org/10.62051/ijcsit.v8n1.09
Journal homepage: https://wepub.org/index.php/IJCSIT/index

Mode-coupled Interferometric Multiparameter Measurement Sensor Based on A Dual Microfiber Ring

Jiali Du, Jiaqi Fan, Chao Feng, Minfei Guo

College of Electrical and Information Engineering, Northeast Petroleum University, Daqing 163318, China

ABSTRACT

A sensor based on dual microfiber ring mode-coupling interference is proposed, which enables simultaneous measurement of temperature and pressure by exploiting mode-coupling interference in bent optical waveguides within dual microfiber rings. The sensor is fabricated by winding microfibers into a dual-ring structure through van der Waals and electrostatic forces. This design not only renders the device compact but also allows the dual-ring structure to realize complex functions within limited space while enhancing sensitivity, making it suitable for integrated applications. Experimental results demonstrate that the sensor achieves a temperature sensitivity of –2.4033 nm/°C and a pressure sensitivity of –4.8863 dBm/kPa. Owing to its distinct response mechanisms to external temperature and pressure variations, the sensor allows simultaneous demodulation of temperature and pressure. Furthermore, the sensor is highly responsive to minute signal changes, making it suitable for real-time monitoring of temperature and stress variations in production lines, thus providing early warning of potential failures and reducing safety risks. With its compact structure and high sensitivity, the proposed microfiber sensor holds great promise for emerging applications in the field of sensing technology.

KEYWORDS

Dual microfiber ring; Mode-coupled interference; Temperature measurement; Pressure measurement

1. INTRODUCTION

Technological innovation has promoted the widespread application of sensors [1]. Microfibers have become an ideal platform for multiparameter sensing due to their small size, strong light-matter interaction, and excellent optical properties. By optimizing the structure and coupling mechanisms, the evanescent field can be enhanced, improving interaction efficiency with the external environment and thereby increasing sensor sensitivity and response speed [2]. Although progress has been made in measuring single parameters such as temperature [3, 4], pressure [5, 6], water hardness [7], stress [8], and underwater acoustic signals [9], simultaneous multiparameter sensing still faces challenges. Current research primarily focuses on optimizing individual parameters, which struggles to meet the demand for high-precision synchronous measurements in complex environments. In fields such as environmental monitoring, smart healthcare, and real-time engineering monitoring, high-precision sensors capable of simultaneously detecting multiple parameters—including temperature, pressure, strain, and refractive index—hold significant value.

In recent years, the demand for multiparameter sensing has driven the development of simultaneous detection technologies. Representative achievements include: a seawater temperature-pressure sensor [10], a single microfiber tactile sensor [11], and a temperature-pressure sensor based on a dual-

interference microfiber resonator [12]. By optimizing the fiber structure and coupling mechanisms, these technologies demonstrate excellent multiparameter sensing capabilities, providing feasible solutions for real-time monitoring in complex environments.

Given the significant application value of multiparameter measurement sensors, this paper proposes a sensor design based on dual microfiber ring mode-coupling interference. The aim is to optimize the microfiber geometry and coupling mechanisms to provide a new approach for mitigating cross-sensitivity in multiparameter measurements, thereby enabling efficient simultaneous monitoring of temperature and pressure.

2. THEORY OF OPERATION

The schematic representation of the sensor is illustrated in Fig.1(a). The sensor is constructed from single-mode fiber (SMF), which is transformed into a microfiber using a hot-melt stretching technique. Subsequently, the produced microfiber is coiled to create a double-ring configuration, relying on van der Waals and electrostatic forces, as depicted in Fig.1(b), $r_1 \neq r_2$.

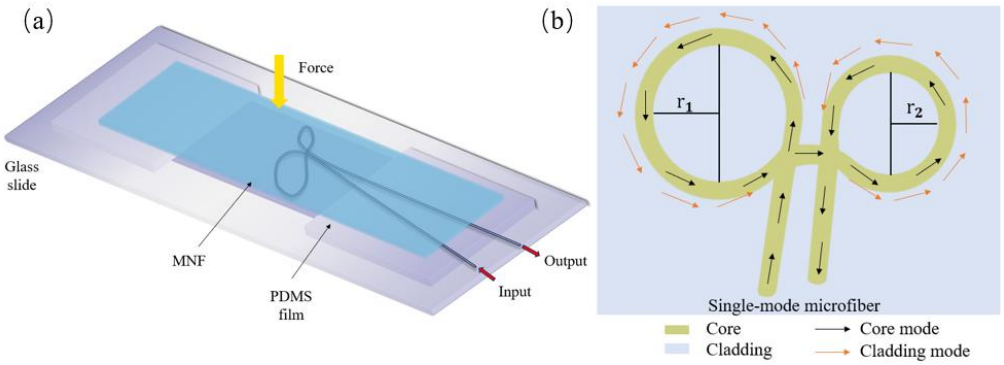

Figure 1. (a) Schematic diagram of the sensor structure. (b) Sensor mode analysis diagram

As indicated in Fig.1(b), light from the source enters the ring with a radius r1 in the fundamental mode along the fiber. The reduction in core radius, combined with the bending of the waveguide, diminishes the core's ability to confine the signal light as the fiber diameter decreases beyond a certain threshold. This phenomenon leads to the excitation of higher-order leakage modes, resulting in a portion of the signal light escaping from the core and manifesting as cladding light. Furthermore, the polydimethylsiloxane (PDMS) material exhibits favorable optical properties in the mid-infrared spectral range, facilitating light leakage into the PDMS cladding, which in turn excites cladding modes. When the light traverses the bent waveguide again, a fraction of it is re-coupled into the fiber core, leading to interference due to the disparity in effective refractive indices between the core and the PDMS cladding, as well as the variation in the optical path length encountered by the incident light. This interference is reiterated when the light subsequently enters the ring of radius r2. For mode-coupled interference, the output intensity can be mathematically represented as [13].

$$I = I_{re} + I_{ad} + 2\sqrt{I_{re} + I_{ad}} \cos\left(\frac{2\pi L\, \Delta n_{eff}}{\lambda}\right) \tag{1}$$

Where I_{re} signifies the intensity of the core mode of the microfiber, I_{ad} represents the intensity of the cladding mode of the PDMS, Δn_{eff} denotes the effective refractive index difference between the core and cladding modes, L indicates the effective interference length, and λ is the wavelength of light in a vacuum. When the condition c is odd, the central wavelength of the interference dip can be expressed as [14].

$$\lambda_c = \frac{2\Delta n_{eff}}{2c+1} \tag{2}$$

According to Fig. 1(b), since $r_1 > r_2$, the effective interference length satisfies $L_1 > L_2$. Light propagates for a longer duration in the ring with a radius of r_1, leading to an increased optical path difference. Denoting the optical path difference as Δ, we have:

$$\Delta = L\Delta n_{eff} \tag{3}$$

The spectral transmission characteristics of the sensor are influenced by the incident wavelength λ, interference length L, microfiber radius r, and the refractive index of the PDMS cladding layer n_3. When temperature and pressure change, PDMS, serving as a sensitive layer, undergoes refractive index variations (n_3), simultaneously affecting the structural parameters of the microfiber (r, L). These changes modulate the interference spectrum period, resulting in variations in the reflection spectrum. By monitoring the shift of characteristic wavelengths, dual-parameter measurement of temperature and pressure can be achieved.

Typically, the response of wavelength to temperature can be characterized by dλ/dT, which quantifies the spectral shift caused by minor temperature variations, thereby indicating the sensor's temperature sensitivity. The sensor's temperature response sensitivity can be expressed as:

$$S_T = \frac{d\lambda}{dt} = -\frac{\partial\lambda}{\partial\varphi} \cdot \left(\frac{\partial\varphi}{n_3} \cdot \frac{dn_3}{dt} + \frac{\partial\varphi}{\partial L} \cdot \frac{dL}{dt} + \frac{\partial\varphi}{\partial r} \cdot \frac{dr}{dt} \right) \tag{4}$$

Additionally, the sensor converts external pressure variations into slight micro-bending, causing light originally confined within the core to partially couple into the cladding, thereby reducing the output optical intensity. By simultaneously monitoring changes in interference wavelength and optical intensity, it is possible to effectively distinguish spectral variations induced by temperature and pressure, providing a novel approach to addressing the cross-sensitivity issue in multi-parameter measurements.

3. EXPERIMENTAL AND RESULTS

3.1. Sensor Fabrication

The fabrication process of the sensor is as follows: First, a Corning single-mode fiber with a core diameter of 8 μm and a cladding diameter of 125 μm is tapered to a diameter of 2 μm and a length of 50 mm in the waist region using a heat-melting and drawing process, forming a microfiber. Subsequently, 2 ml of the prepared PDMS is applied to a mold and cured on a hot plate to form a PDMS film with a thickness of 300 μm. Next, the microfiber is coiled into a double-ring structure (r_1 = 4 mm, r_2 = 3 mm), placed on the surface of the PDMS film, and covered with another layer of PDMS to secure the structure.

3.2. Experimental Procedure and Result

The temperature and pressure measurements were performed after sensor fabrication, and the experimental setup is shown in Fig. 2. A broadband light source (NI PXI-4844, 1510–1590 nm) and an optical spectrum analyzer (OSA) were used to evaluate the sensor performance. The spectrometer provides a wavelength sampling interval of 4 pm, a stability of 1 pm, and a resolution of 1 nm. Light emitted from the broadband source propagates through the optical fiber to the microfiber sensing region, where modal interference occurs. For temperature measurements, the sensor was placed inside a thermostatic chamber (SDLS 303-00A) to precisely control the ambient temperature.

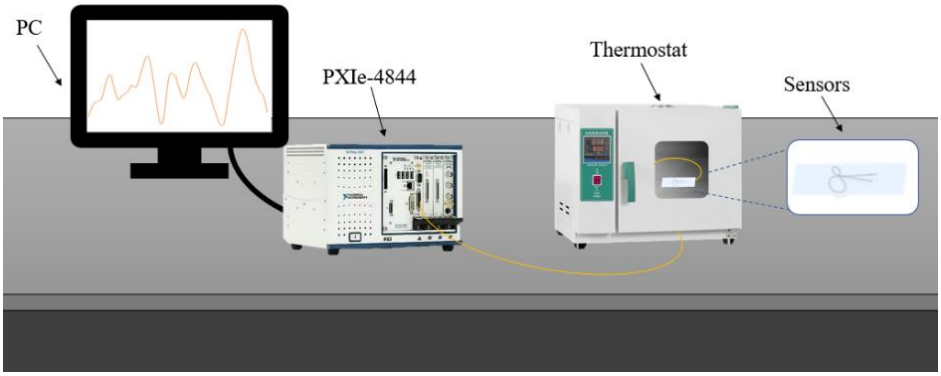

Figure 2. Diagram of the device for measuring the temperature by the sensor

In the temperature performance testing experiment, a thermostatic chamber was used to regulate the sensor's temperature to evaluate its thermal response characteristics. The sensor was placed inside the chamber, and the temperature was gradually increased from 36°C to 37°C in increments of 0.1°C while simultaneously recording the corresponding changes in the reflection spectrum.

Fig. 3(a) presents the reflection spectra at different temperatures. It can be observed that as the temperature increases, the reflection spectrum exhibits a significant blue shift in the wavelength domain, indicating that the optical characteristics of the sensor are highly sensitive to external temperature variations. Further analysis of the relationship between spectral shift and temperature variation is shown in Fig. 3(b), which provides a linear fitting curve of wavelength shift versus temperature change.

Based on the reflection spectrum data and the linear fitting results, the temperature sensitivity of the sensor is calculated to be -2.4033 nm/°C, with an overall fitting error of less than 2.4%. These results demonstrate that the sensor exhibits high sensitivity and a linear response in temperature measurements, making it suitable for high-precision temperature sensing applications.

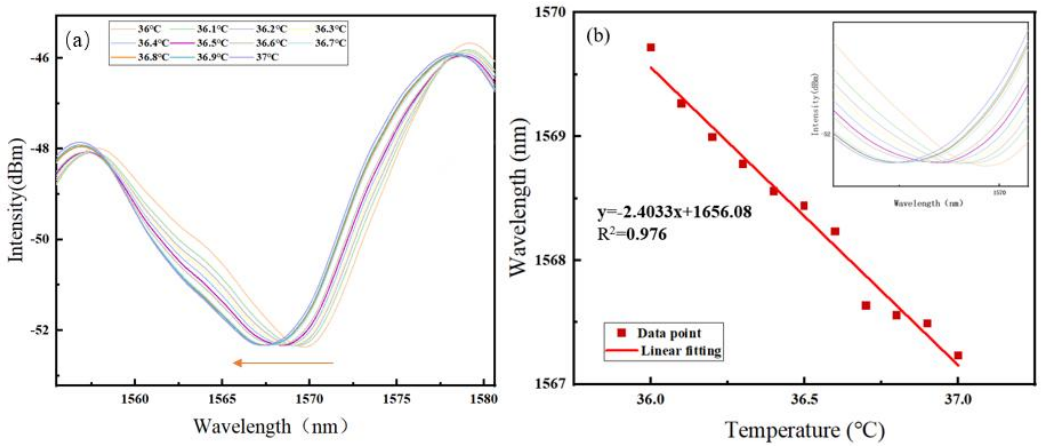

Figure 3. Spectral measurements (a) Measurements at different temperatures (b) Linear fitting results of spectral migration vs. temperature change

In the pressure measurement experiment, the applied pressure on the sensor was gradually varied while recording the corresponding changes in the reflection spectrum. The pressure was adjusted within a range of 0.1 kPa to 0.6 kPa, with a step size of 0.1 kPa.

Fig. 4(a) presents the reflection spectra under different pressure levels. It can be observed that as the pressure increases, the overall intensity of the reflection spectrum shows a decreasing trend. Further analysis of the relationship between spectral shift and pressure variation is shown in Fig. 4(b), which provides a linear fitting curve of spectral shift versus pressure change.

Based on the reflection spectrum data and the linear fitting results, the pressure sensitivity of the sensor is calculated to be -4.8863 dBm/kPa, with an overall fitting error of less than 1.4%. These results indicate that the sensor exhibits high sensitivity and a well-defined linear response in pressure measurements, making it suitable for high-precision pressure sensing applications.

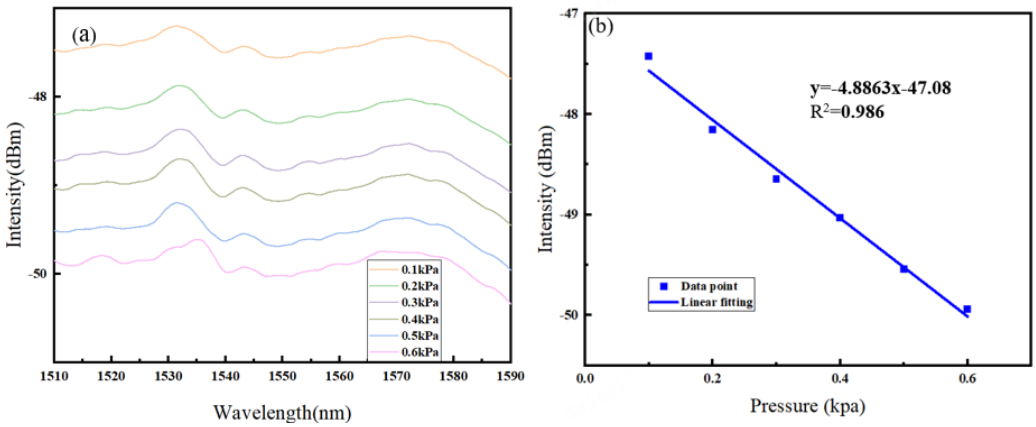

Figure 4. Spectral measurements (a) Measurements at different pressures (b) Linear fit of spectral migration to pressure change

4. CONCLUSION

This paper proposes a multiparameter sensor based on dual microfiber ring mode-coupling interference. By exploiting the distinct responses of the sensor to temperature and pressure variations, simultaneous measurement of temperature and pressure is achieved. Experimental results demonstrate that the sensor's spectral response exhibits regular variations consistent with theoretical expectations when external temperature and pressure change. Specifically, the sensor achieves a temperature sensitivity of -2.4033 nm/°C and a pressure sensitivity of -4.8863 dBm/kPa. In addition, the sensor features compact size, low loss, flexibility, high sensitivity, and multifunctionality, making it particularly suitable for miniaturized or integrated applications such as optical communication, sensing technology, and medical diagnostics, thereby demonstrating significant application potential.

REFERENCES

[1] Y. Shao, S. Du, and D. Huang, "Advancements in Applications of Manufacturing and Measurement Sensors," Sensors 25(2), 454 (2025).

[2] H. Dang et al., "Sensing performance improvement of resonating sensors based on knotting micro/nanofibers: A review," Measurement 170, 108706 (2021).

[3] S. Wang et al., "A High-Sensitivity Temperature Sensor Based on a Liquid Cladding Tapered Microfiber," IEEE Sens. J. 21(5), 6152–6157 (2021).

[4] M. Wang et al., "PDMS-assisted graphene microfiber ring resonator for temperature sensor," Opt. Quantum Electron. 50(3) (2018).

[5] K. Meng et al., "Wearable Pressure Sensors for Pulse Wave Monitoring," Adv. Mater. 34(21) (2022).

[6] C. Jiang et al., "Flexible wearable microfiber respiratory sensor based on microspheres coupling," IEEE Sens. J. 23(22), 27324–27330 (2023).

[7] Y. Niu et al., "High-sensitivity microfiber interferometer water hardness sensor," Measurement 201(6) (2022).

[8] A. Hanif et al., "A Stretchable and Strain-Limiting, Bio-Inspired Nanofiber-Reinforced Microfiber for Wearable Electronics," Adv. Mater. Technol. 9(4) (2023).

[9] Z. Zhang et al., "A Multifunctional Airflow Sensor Enabled by Optical Micro/Nanofiber," Adv. Fiber Mater. 3(6), 359–367 (2021).

[10] X. Zhai et al., "Underwater acoustic sensor based on microfiber knot resonator," Opt. Fiber Technol. 84 (2024).

[11] N. Yao et al., “Single optical microfiber enabled tactile sensor for simultaneous temperature and pressure measurement,” Photonics Res. 10(9) (2022).

[12] L. Wei et al., “Integrating Interference and Resonance Effects in Microfiber Sensors for Simultaneous Pressure and Temperature Measurement,” IEEE Sens. J. 1, 1–1 (2024).

[13] C. Lee et al., “Wavelength measurement by Fourier analysis of interference fringes through a plane parallel plate,” Appl. Opt. 56(9), 9638–9643 (2017).

[14] H. Y. Choi, M. J. Kim, and B. H. Lee, “All-fiber Mach-Zehnder type interferometers formed in photonic crystal fiber,” Opt. Express 15, 5711–5720 (2007).

[15] Y. F. Hou, J. Wang, and X. Wang, “Simultaneous Measurement of Pressure and Temperature in Seawater with PDMS Sealed Microfiber Mach-Zehnder Interferometer,” J. Lightwave Technol. 38(22), 6412–6421 (2020).